INTERNATIONAL SOCIETY FOR SOIL MECHANICS AND GEOTECHNICAL ENGINEERING

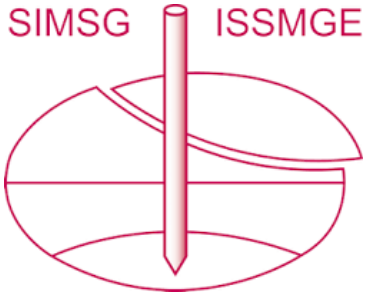

This paper was downloaded from the Online Library of the International Society for Soil Mechanics and Geotechnical Engineering (ISSMGE). The library is available here:

https://www.issmge.org/publications/online-library

This is an open-access database that archives thousands of papers published under the Auspices of the ISSMGE and maintained by the Innovation and Development Committee of ISSMGE.

The paper was published in the proceedings of the 20th International Conference on Soil Mechanics and Geotechnical Engineering and was edited by Mizanur Rahman and Mark Jaksa. The conference was held from May 1st to May 5th 2022 in Sydney, Australia.

Proceedings of the 20th International Conference on Soil Mechanics and Geotechnical Engineering– Rahman and Jaksa (Eds)
© 2022 Australian Geomechanics Society, Sydney, Australia, ISBN 978-0-9946261-4-1

The effects of gradation on the dynamic response of embankments

Les effets de la gradation sur la réponse dynamique des remblais

Trevor J. Carey
Department of Civil Engineering, The University of British Columbia, Vancouver, BC, Canada,
Trevor.Carey@ubc.civil.ca

Jason T. DeJong, Katerina Ziotopoulou, & Alejandro Martinez
Department of Civil and Environmental Engineering, University of California at Davis, Davis, CA, USA,

Anna Chiaradonna
Department of Civil, Construction, Architectural, and Environmental Engineering, University of L'Aquila, L'Aquila AQ, Italy

ABSTRACT: The standard of practice when assessing the seismic performance of well graded sands, is to assume the response is similar to poorly graded clean sands, which comprise the majority of the liquefaction case history database. Using the 9-m radius centrifuge at UC Davis, an experiment was designed to elucidate the system-level liquefaction triggering response for a poorly graded and well graded sand. The experiment consisted of two identical 10-degree slopes positioned side-by-side in the same model container, with one slope constructed with a well graded sand and the other with a poorly graded sand. The D_{10} grain size was the similar for both gradations and therefore the permeability was comparable. The slopes were dry pluviated to the same relative density of D_r=63%, while the absolute densities were different. The dynamic response of both slopes was similar up until liquefaction triggering, with both sands reaching excess pore pressure ratios close to unity within 1-2 cycles of loading. Following the onset of liquefaction, the well graded sand exhibited strong dilative tendencies and embankment deformations attenuated rapidly during successive loading cycles, while the poorly graded sand embankment continued to deform. This study demonstrates that the post-triggering response of well graded and poorly graded sands differ due to their different absolute densities and dilatancies for the same relative density. It is expected that findings from this research will lead to a more rational accounting of gradation properties in the evaluation of and design for liquefaction effects, as well as the interpretation of case histories.

RÉSUMÉ : La pratique courante de l'évaluation de la performance sismique des sables bien classés est de supposer que la réponse est similaire à celle des sables mal classés, qui constituent la majorité des cas historiques. En utilisant la centrifugeuse de 9 m de rayon à UC Davis, une expérience a été conçue pour clarifier la réponse de déclenchement de liquéfaction pour un sable mal classé et un sable bien classé. L'expérience consistait de deux pentes identiques de 10 degrés placées une à côté de l'autre dans le même conteneur, avec une pente construite avec un sable bien classe et l'autre avec un sable mal classé. D_{10} était le même pour les deux gradations et donc la perméabilité était la même. Les pentes avaient la même densité relative de D_r = 63%, tandis que la densité absolue était différente. La réponse dynamique des deux pentes était similaire jusqu'au déclenchement de la liquéfaction, avec les deux sables atteignant des excès de pression interstitielle en 1 à 2 cycles de chargement. Après le déclenchement de la liquéfaction, le sable bien classé présentait de fortes tendances dilatives et ses déformations s'atténuaient rapidement au cours des cycles de chargement successifs, tandis que le sable mal classé présentait des déformations continuellement croissantes. Cette étude démontre que la réponse post-déclenchement des sables bien classés diffère des sables mal classés en raison de leurs différentes densités absolues et dilatances pour une densité relative commune. On s'attend à ce que les résultats de cette recherche conduisent à une comptabilisation plus rationnelle des propriétés de granulation dans l'évaluation et la conception des effets de liquéfaction, ainsi que dans l'interprétation des cas historiques.

KEYWORDS: Liquefaction, centrifuge testing, well-graded soil, embankment, dynamic performance

1 INTRODUCTION

The liquefaction triggering analysis procedure uses an empirical case history database that was primarily developed from observations at sites consisting of relatively clean poorly graded sands. However, more broadly graded soils are found in the built environment, requiring engineering evaluation of soils that fundamentally differ from the database of sands used to develop the basis of understanding and design methods. This knowledge gap has led to the assumption that the dynamic behavior of poorly graded sands is roughly comparable to well graded sands, which implies that relative changes in gradation characteristics such as initial void ratio (e) or coefficient of uniformity (C_u) have negligible effects on dynamic soil behavior.

Sturm (2019) developed a level ground centrifuge experiment test program to investigate the effects of earthquake shaking on the liquefaction triggering and post liquefaction volumetric reconsolidation strains using a suite of sands with D_{50} particle grain sizes ranging from 0.2 to 2.6 mm, which had C_u values from 1.7 to 7.4. Liquefaction was triggered for each sand, but as C_u increased lower volumetric strains were measured. Sturm (2019) attributed the lower strains to the well graded sands having a larger G_{max}, lower initial void ratios, and stronger stress-dilatancy tendencies.

This paper describes a centrifuge experiment that was designed to elucidate the effect that sand gradation has on system-level performance of embankments. The experiment was conducted at the UC Davis Center for Geotechnical Modeling (CGM) using the 9-m radius centrifuge and consisted of two submerged embankments positioned side-by-side in the same rigid model container, with one embankment constructed with a poorly graded sand, and the other with a well graded sand. Both embankments were dry pluviated to the same relative density of D_r=63%, however the absolute density for the well graded embankment was larger. To track acceleration and porewater

pressure responses in each embankment during shaking, vertical arrays of sensors were located beneath the level ground at the head of the slope and in the mid-slope. The input container motion used to simulate earthquake shaking consisted of a non-uniform 20 cycle, 1 Hz sinewave. Stress-strain responses were computed using inverse analysis approaches for both the level and sloping ground conditions for both gradations. This experiment demonstrates that poorly and well graded sands have different dynamic behaviors.

2 SOILS AND TEST DESIGN

The grain size distributions of the two test sands used for this study are illustrated in Figure 1. The well graded sand, 25ABCD, has a C_u of 7.45 and the C_u of the poorly graded sand, 100A, is 1.68. The D_{50} of the 100A and 25ABCD sands are 0.18 and 1.21 mm, respectively. The e_{max} and e_{min} index properties of the sands are provided in Table 1, along with the void ratios at the test relative density of D_r=63%. The two sands were mined from the same Cape May Formation near Mauricetown, New Jersey, and have similar mineralogy and shape characteristics (Sturm 2019). The hydraulic conductivity was measured using a falling head permeability test in the laboratory at the D_r=63% test condition, with k=0.02 cm/sec measured for the 100A sand and k=0.01 cm/sec for the 25ABCD sand.

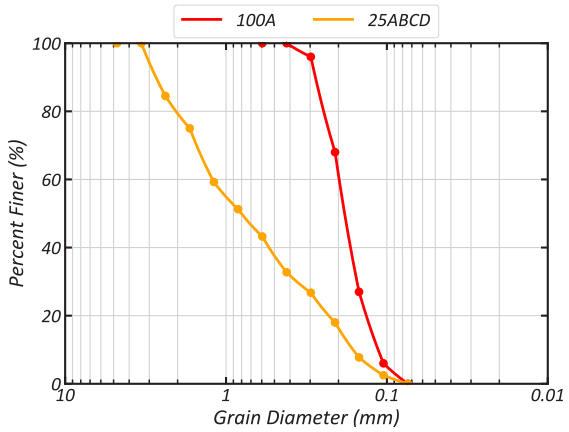

Figure 1. Grain size distributions of the two test sands.

The experiment consists of two identical submerged 10-degree embankments positioned side-by-side in a rigid model container. Positioning the embankments side-by-side ensured the ground motion was applied with the same polarity to the embankments. The experiment was performed on the 9 m radius centrifuge at the UC Davis CGM at a centrifugal acceleration of 40 g, with a pore fluid viscosity (μ*) 40 times that of water. Conventional centrifuge scaling laws for gravity were followed (Garnier et al. 2007).

Table 1. Key index properties of the two test sands.

Sand	e_{min}	e_{max}	e @ D_r=63%	D_{50} (mm)	C_u
100A	0.579	0.881	0.69	0.18	1.68
25ABCD	0.303	0.544	0.39	0.80	7.44

An elevation view of the centrifuge experiment design is provided in Figure 2. At the centrifugal acceleration of 40 g, each embankment had level ground benches that are 19.8 m in length located at the head and toe of a 30.9 m slope. A rigid aluminum wall separated the embankments into equal widths of 17.75 m. A base layer of dense sand (D_r>90%) was used to elevate the embankments so they were visible through the transparent model container sidewalls for recording with high-speed cameras. Each embankment was instrumented with two vertical arrays of sensors consisting of accelerometers (shown as triangles) and porewater pressure transducers (circles). The sensor arrays were located beneath the level ground at the head of the slope and in the mid-slope. The accelerometer and porewater pressure transducers were located at equivalent depths from the ground surface in the two arrays, and therefore alike sensors have similar initial vertical effective stresses. The embankments were constructed sequentially using dry pluviation in 2.5 cm lifts, matching the vertical spacing between accelerometers and porewater pressure transduces.

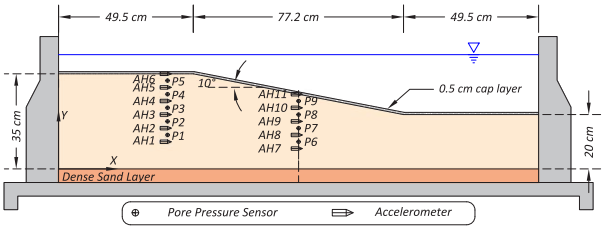

Figure 2. Elevation view of the testing schematic in model scale units. Embankment design is identical for both the 100A and 25ABCD sands.

The sequence of motions used to simulate earthquake shaking consisted of four, 1-Hz sinewave motions of increasing shaking intensity. Each input motion had the same topology of a linear ramp of cycles with increasing acceleration, multiple constant amplitude cycles at a desired peak acceleration, and an exponential decay of acceleration. The shape of the input motion was chosen to avoid sudden starts and stops in shaking and to have an energy distribution more typical of recorded earthquake motions.

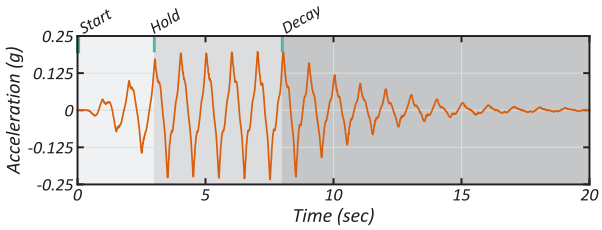

Figure 3. Motion used to simulate earthquake shaking.

The recorded input motion, applied at the model container base, for the third shake of the shaking sequence is presented in Figure 3. The background shading of the figure indicates the linear ramp of acceleration occurring over 3 cycles, the 5 hold cycles at a PGA of 0.23 g, and a 12-cycle exponential decay from the PGA. The results presented herein are for the input motion shown in Figure 3.

The longitudinal sidewalls of the rigid model container were optically clear polycarbonate, which allowed for a cross-sectional view of each embankment. To assess liquefaction-induced deformations along each cross-section, a series of high-contrast, black vertical sand columns were installed at 10 cm intervals. The columns were manufactured and attached to the container sidewalls using water soluble glue and were installed prior to pluviation of the embankments. The water-soluble glue softened during saturation allowing the columns to deform with the embankments. Positioned on the exterior of the model container, along each sidewall, were 3 high-speed cameras (6 cameras total) recording the deforming embankments and black sand columns at 1,000 frames per second during shaking.

GeoPIV-RG (Stanier et al. 2015) was used to convert videos of the deforming centrifuge experiment to displacement time-histories. The GeoPIV procedure subdivides an initial image of the embankment cross-section into a series of circular image patches and tracks the patch locations through sequential images of embankment deformation. The black sand columns were tracked using 60 pixel diameter patches that were spaced vertically every 20 pixels to ensure full coverage of each column. Permanent embankment displacements calculated using GeoPIV are used to evaluate how embankment deformations differs for the two test sands.

3 RESULTS

Level Ground Conditions: In Figures 4 and 5 the input motion, recorded accelerations for AH4, AH5, AH6, excess porewater pressures for P4 and P5, and the dynamic stress-strain for the 100A and 25ABCD embankments are provided. The dashed lines in the porewater pressure figures correspond to the excess porewater pressure at that sensor depth that is equivalent to an excess porewater pressure ratio (r_u) of 1.0. The dynamic stress-strain responses were computed using inverse analysis approaches, with stresses calculated using the procedure recommended by Kamai & Boulanger (2010), and shear strains calculated using the weighted residual method described by Brandenberg et al. (2010). The inverse analysis approach assumes a pseudo-element is located between accelerometer pairs, with stresses and strains calculated at the midpoint of these elements. For example, pseudo-element Ele 5-6 and 4-5 are calculated between AH5-AH6 and AH4-AH5 respectively. The color gradient in the stress-strain and excess porewater pressure figures are correlated in time for comparison of the two responses.

The 1 Hz frequency and topology of the base input motion was better preserved in the 25ABCD embankment. Both positive and negative accelerations are maintained over the entire array of sensors. As the motion propagated upwards through the 25ABCD array it is amplified and de-liquification dilation spikes are observed, a behavior described by Kutter and Wilson (1999) where upward propagating shear waves are transformed into a sharp wave front due to differences in soil stiffness from dilation.

As the input motion propagated to the ground surface in the 100A embankment it became progressively more attenuated and the soil was unable to transfer negative accelerations. At the AH6 sensor, the soil softened to the extent during liquefaction it is unable to propagate any accelerations, effectively isolating the upper portion of the soil column from the input motion.

Excess porewater pressures built rapidly in both embankments and liquefaction was triggered (r_u=1.0) at each porewater pressure transducer. However, the generation of excess porewater pressures was quicker in the 100A embankment. Both P4 and P5 in the 100A model reached a r_u of 1.0 at about 5 seconds, prior to the constant amplitude cycles of the input motion. For the 25ABCD embankment, liquefaction was triggered at about 6 seconds at P5 and 8 seconds at P4. The delayed generation of excess porewater pressures in the 25ABCD embankment occur even with a lower permeability.

The 25ABCD embankment had large drops and rebounds in excess porewater pressure as the sand dilated during loading. The reduction of excess porewater pressures occurs prior to the triggering of liquefaction (i.e., P5) at a frequency of 0.5 Hz, suggesting that dilation occurs in both the downslope and upslope directions of acceleration. The momentary reduction in excess porewater pressures stiffens the soil column, which reduces instability and deformation. Dilation in the 100A embankment was more subdued with lower magnitudes and less frequent drops in excess porewater pressure.

The dynamic stress-strain figures corroborate the behavior observed in the acceleration and excess porewater pressure responses. The maximum dynamic strain recorded in the 100A embankment at the pseudo-element Ele 5-6 was roughly 3.25%. The flat CSR response is an indication the soil column has softened and is unable to transmit shear stresses. Larger shear stresses and lower shear strains occur in the pseudo-element Ele 4-5.

For the 25ABCD embankment, the maximum dynamic shear strain was about 1% for both elements. Dilation in the stress-strain response was observed for both the positive and negative accelerations, which were consistent with the recorded dilation spikes in the acceleration and porewater pressure responses.

Mid-Slope Ground Conditions: In Figures 6 and 7 an analogous figure set to the level ground conditions (Figures 4 and 5) is given for the vertical array of sensors located in the mid-slope. The 10-degree slope imposed an initial static shear stress that affects the dynamic response of the soil in the slope (Idriss and Boulanger 2008).

Large magnitude positive downslope acceleration spikes occurred in both embankments as each sand dilated during loading, with the spikes being larger in the 100A embankment. It is hypothesized the spikes are larger for the 100A embankment because stronger dilatancy was mobilized due to the higher severity of liquefaction caused by more rapid decreases in initial confining stress. The porewater pressure measurements indicate the 25ABCD embankment briefly liquified at P8, but with a limited number of loading cycles at low effective stress conditions implies that a strong dilative response was not mobilized. Despite the presence of an initial static shear stress, which produces unsymmetrical loading and preferential downslope straining, the 25ABCD sand maintained minor dilation spikes as the soil is loaded in the upslope direction.

Liquefaction was triggered in both embankments at the P9 and P8 sensors, but pore pressures began to dissipate prior to the end of shaking. Following shaking, at 22 seconds, the r_u values in both embankments decreased to about 0.5, suggesting the slopes were not completely undrained during loading.

The dynamic stress-strain response for the 100A embankment has a clear downslope bias in the direction of the static shear stress. The upslope dilation in the acceleration response for the 25ABCD embankment was evident by the negative CSRs. Both embankments reached a similar level of dynamic strain of roughly 2%, however given the initial static stress the permanent shear strains are expected to be larger.

Embankment Displacements: The permanent horizontal displacements of the black sand columns at the end of shaking calculated using GeoPIV and the high-speed videos are presented in Figure 8 with the embankment geometry. Displacements at each patch location are shown using quiver arrows, and a quiver corresponding to 1 m of displacement is provided for reference at the top of the figure. The displacements in Figure 8 are incremental and do not include accumulated displacements from the proceeding shaking events.

The displacement trends in Figure 8 follow expected patterns, with the largest magnitudes occurring mid-slope as that is least affected by the level ground conditions at the terminus of the slope. Of the two embankments, displacements are larger throughout the 100A embankment. The mid slope displacement (at 34 m) is 0.3 m and 0.08 m for the 100A and 25ABCD embankments, respectively.

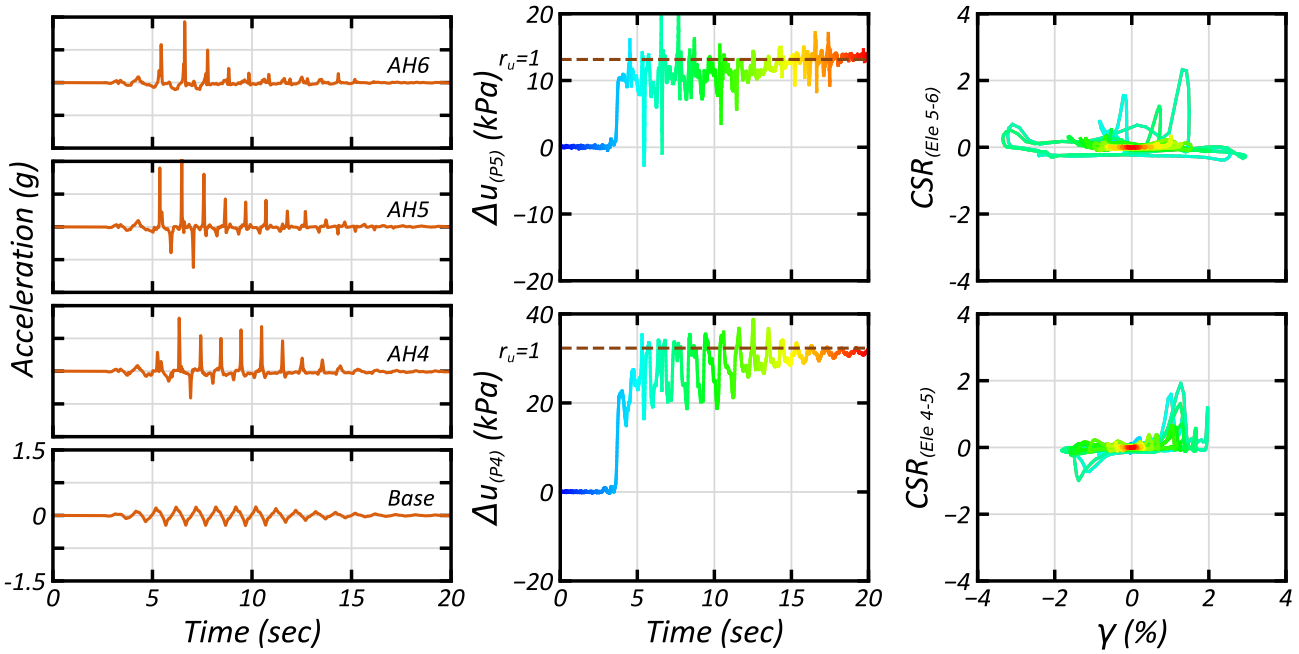

Figure 4: Dynamic response of the level ground conditions for the 100A embankment. For left to right, (left column) acceleration response, (middle column) excess porewater response with excess porewater pressure that corresponds to an r_u=1.0, and (right column) stress strain response of the pseudo-elements. The color gradients in the porewater pressure and stress-strain responses are correlated in time.

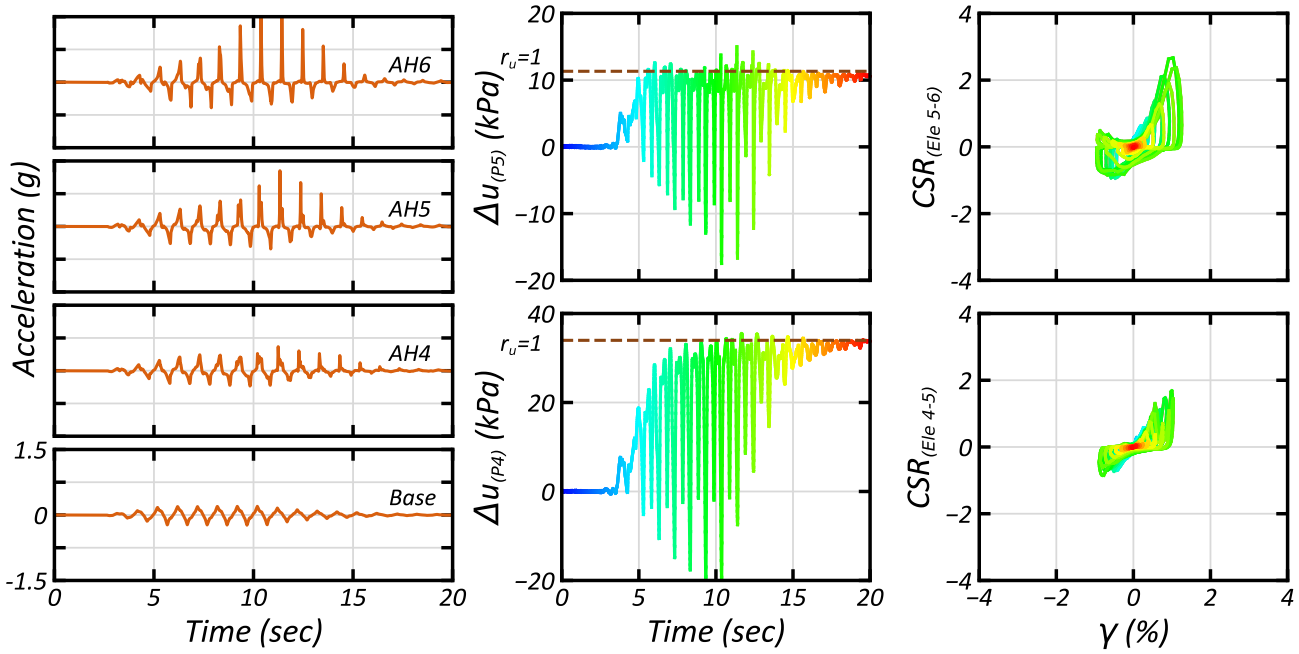

Figure 5: Dynamic response of the level ground conditions for the 25ABCD embankment. For left to right, (left column) acceleration response, (middle column) excess porewater response with excess porewater pressure that corresponds to an r_u=1.0, and (right column) stress strain response of the pseudo-elements. The color gradients in the porewater pressure and stress-strain responses are correlated in time.

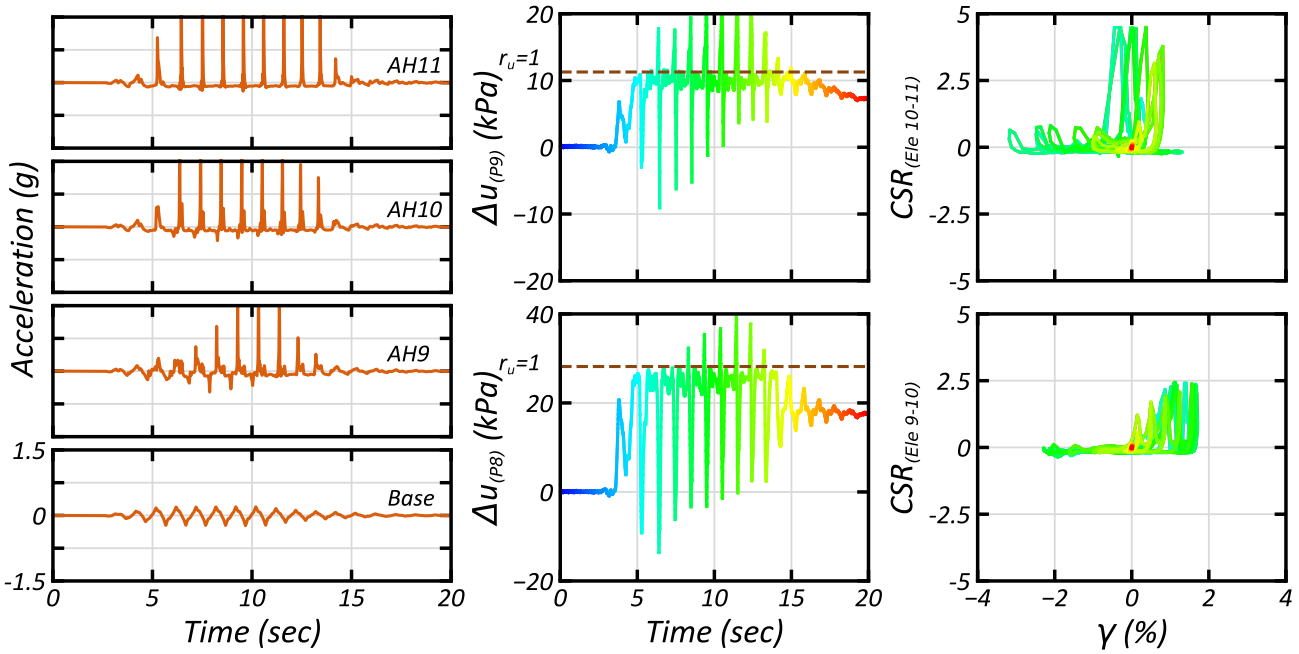

Figure 6: Dynamic response of the mid-slope ground conditions for the 100A embankment. For left to right, (left column) acceleration response, (middle column) excess porewater response with excess porewater pressure that corresponds to an r_u=1.0, and (right column) stress strain response of the pseudo-elements. The color gradients in the porewater pressure and stress-strain responses are correlated in time.

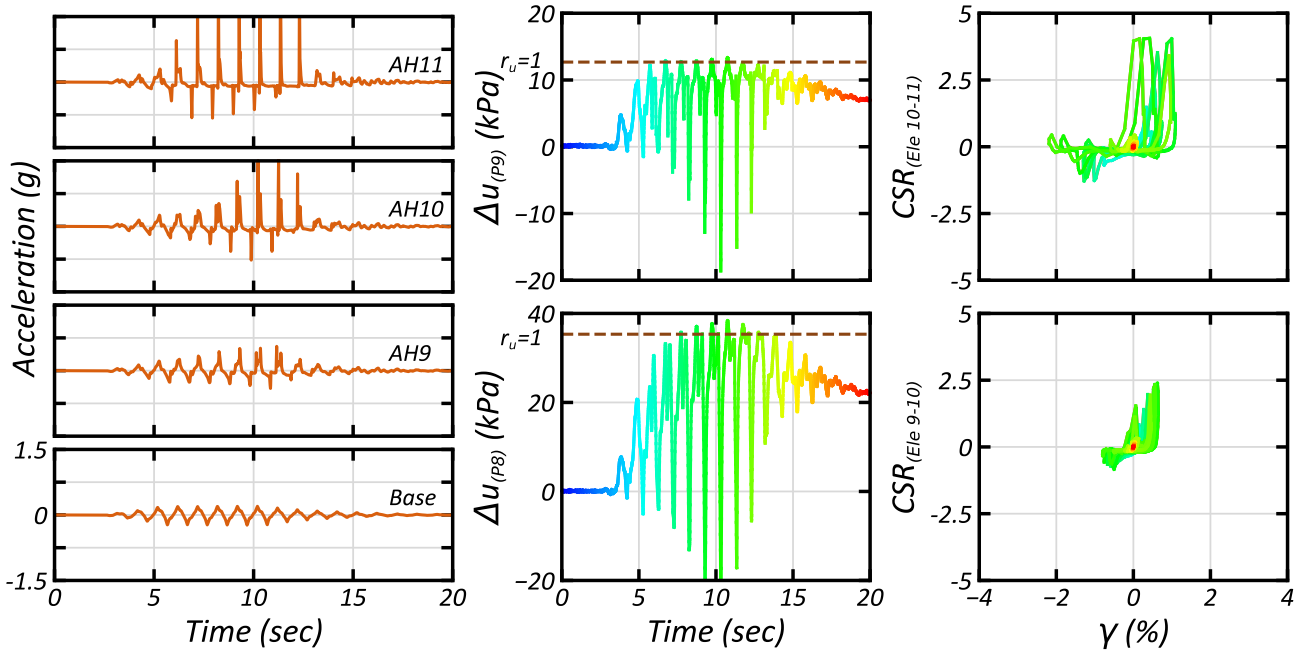

Figure 7: Dynamic response of the mid-slope ground conditions for the 25ABCD embankment. For left to right, (left column) acceleration response, (middle column) excess porewater response with excess porewater pressure that corresponds to an r_u=1.0, and (right column) stress strain response of the pseudo-elements. The color gradients in the porewater pressure and stress-strain responses are correlated in time.

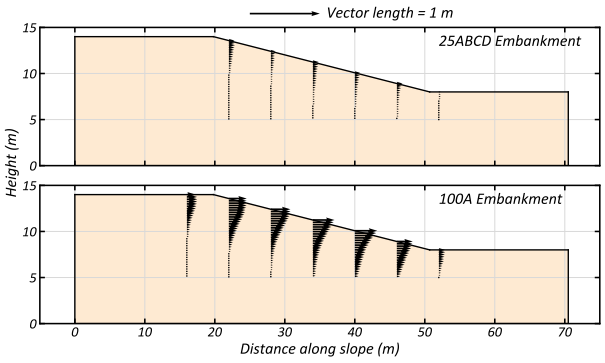

Figure 8. Horizontal displacements of each embankment calculated using the high-speed video recordings and GeoPIV

4 DISCUSSION

The dynamic responses of the sands in Figures 4 to 7 demonstrate the poorly graded 100A and well graded 25ABCD sands fundamentally differ in their response to dynamic loading. Excess porewater pressure measurements indicate liquefaction was triggered in both embankments, and changes in the frequency content and the presence of dilation spikes observed in the in-situ acceleration recordings is further evidence of liquefaction. However, the post triggering deformation response for the embankments bifurcates, and the 25ABCD embankment has a mid-slope displacement that is about 75% less than the displacement measured in the 100A embankment. It is hypothesized that the lower displacements in the 25ABCD embankment is from the slower generation and faster dissipation of excess porewater pressures, coupled with the stronger stress-dilatancy behavior, reducing embankment instability. Stronger stress-dilatancy behavior in the 25ABCD embankment is supported by both the acceleration and excess porewater pressure responses.

Current analysis procedures assume an expected level of shear straining at triggering of liquefaction (i.e., r_u=1.0, γ=3%), and frequently these definitions of liquefaction are used interchangeably (Idriss and Boulanger 2008). It is reasonable to expect that the well graded sand also has an expected level of accumulated shear strains at triggering, but the magnitudes of strains are lower than the γ=3%, commonly assumed to be coincident with r_u = 1.0 for poorly graded sands.

The displacements measured in the 100A embankment are a closer representation of what would be predicted using the empirical case history database, since the poorly graded 100A sand is similar to many of the soils that comprise the database. Comparing the embankment responses herein demonstrates that the current liquefaction analysis procedures may produce overly conservative embankment performance estimates for systems constructed with well graded sands, and that poorly graded sands do not accurately represent the dynamic behavior of well graded sands.

5 CONCLUSIONS

A centrifuge experiment was performed to elucidate how sand gradation effects the system-level performance of embankment structures during earthquake shaking. The experiment consisted of two embankments positioned side-by-side in a rigid model container, with one constructed with a clean poorly graded sand and the other with a well graded sand. The following are the observations can be made:

Liquefaction can be triggered in poorly graded and well graded sands, but the embankment constructed with the well graded sand (25ABCD) will have stronger stress-dilatancy behavior, stiffening the model pre and post triggering of liquefaction (r_u = 1.0).

- The embankment constructed with the 25ABCD sand had greater resistance to the generation and faster dissipation of excess porewater pressures, even with a lower permeability.
- The stress-strain responses for the level ground array indicate stiffness was maintained in the 25ABCD embankment following liquefaction. This enabled the transmission of shear stresses through the soil column. Once liquefaction was triggered in the 100A embankment, shear stresses were damped out and were not propagated to the ground surface.
- Lower permanent embankment deformations were measured in the embankment constructed with the well graded 25ABCD sand.

This experiment demonstrates that the thoroughly understood dynamic response of relatively clean poorly graded sands does not accurately describe the dynamic behavior of more well graded sands. Other gradation properties should be considered during liquefaction assessment, which may warrant additional studies to fully understand which properties of soil gradation will decrease liquefaction-induced straining. This will produce more rigorous liquefaction analysis procedures for new and existing embankments structures, reducing the likelihood of overly conservative embankment designs.

6 ACKNOWLEDGEMENTS

The National Science Foundation (NSF) provided the funding for this work (Grant No. CMMI-1916152) and for the Natural Hazards Engineering Research Infrastructure (NHERI) centrifuge facility at UC Davis (Grant No. CMMI-1520581). Any opinions, findings and conclusions or recommendations expressed in this material are those of the author(s) and do not necessarily reflect those of the NSF. The authors would also like to thank Dr. Dan Wilson, Rachel Reardon, Francisco Humire, Mandeep Singh Basson, and Sheikh Sharif Ahmed, for their insights and recommendations. The authors would also like to thank the UC Davis CGM staff for their assistance during centrifuge testing.

7 REFERENCES

Brandenberg, S.J., Wilson, D.W. and Rashid, M.M. 2010. A weighted residual numerical differentiation algorithm applied to experimental bending moment data. *Journal of Geotechnical and Geoenvironmental Engineering*, 136, 854-863

Garnier, J., Gaudin, C., Springman, S.M., Culligan, P.J., Goodings, D., Konig, D., Kutter, B., Phillips, R., Randolph, M.F., and Thorel, L. 2007. Catalogue of scaling laws and similitude questions in geotechnical centrifuge modelling. *International Journal of Physical Modelling in Geotechnics*, 7(3), 1–23.

Idriss, I.M. and Boulanger, R.W. 2008. *Soil Liquefaction During Earthquakes*, Oakland, CA, Earthquake Engineering Research Institute.

Kamai, R., and Boulanger, R.W. 2010. Characterizing localization processes during liquefaction using inverse analyses of instrumentation arrays, *Meso-scale shear physics in earthquake and landslide mechanics*, 219-238.

Kutter, B. L. and Wilson., D.W. 1999. De-Liquefaction Shock Waves. *7th US-Japan Workshop on Earthquake Resistant Design of Lifeline Facilities and Countermeasures Against Soil Liquefaction*. Buffalo, NY.

Stanier, S.A., Blaber, J., Take, W.A. and White, D.J. 2015. Improved image-based deformation measurement for geotechnical applications. *Canadian Geotechnical Journal*, 53(5), 727–739.

Sturm, A.P. 2019. On the Liquefaction Potential of Gravelly Soils: Characterization, Triggering and Performance. PhD Dissertation. University of California, Davis.